Asymmetric Effect of Oxygen Adsorption on Electron and Hole Mobilities in Bilayer Graphene: Long- and Short-Range Scattering Mechanisms

Ive Silvestre,[†,⊥] Evandro A. de Morais,[†,‡,⊥] Angelica O. Melo,[†] Leonardo C. Campos,[†] Alem-Mar B. Goncalves,[†,§] Alisson R. Cadore,[†] Andre S. Ferlauto,[†] Helio Chacham,[†] Mario S. C. Mazzoni,[†] and Rodrigo G. Lacerda[†,*]

[†]Departamento de Física, ICEx, Universidade Federal de Minas Gerais-UFMG, C.P. 702, 30123-970, Belo Horizonte, MG, Brazil, [‡]Universidade Federal de Itajubá, Campus avançado de Itabira, Rua Irmã Ivone Drumond, 200-Distrito Industrial II, Itabira, MG, Brazil, and [§]Instituto de Física, Universidade Federal do Mato Grosso do Sul-UFMS, C.P. 549, 79070-900, Campo Grande, MS, Brazil. [⊥]These authors contributed equally.

ABSTRACT We probe electron and hole mobilities in bilayer graphene under exposure to molecular oxygen. We find that the adsorbed oxygen reduces electron mobilities and increases hole mobilities in a reversible and activated process. Our experimental results indicate that hole mobilities increase due to the screening of long-range scatterers by oxygen molecules trapped between the graphene and the substrate. First principle calculations show that oxygen molecules induce resonant states close to the charge neutrality point. Electron coupling with such resonant states reduces the electron mobilities, causing a strong asymmetry between electron and hole transport. Our work demonstrates the importance of short-range scattering due to adsorbed species in the electronic transport in bilayer graphene on SiO_2 substrates.

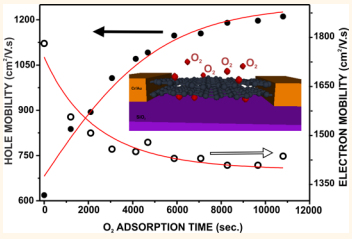

KEYWORDS: graphene · electrical transport · scattering mechanisms · gas interaction

Graphene is a material endowed with a distinctive Dirac-like energy dispersion presenting exotic quantum behavior.[1−4] Shortly, it was soon found out that its electronic properties are strongly sensitive to substrates and its environment, resulting in pronounced changes in charge carrier migration.[5−8] The mechanisms behind the charge scattering processes as well as the limitations of graphene mobility are still hotly debated,[9−12] and a full picture of these phenomena is of central importance since the impact of such scattering centers is a crucial point for electronic applications.[13−16] Curiously, the pursuit for the understanding of electron scattering mechanisms has been mainly focused on monolayer graphene,[17,18] even though bilayer graphene and few-layer graphene also present interesting tunable quantum properties and potential for electronic applications.[19−22]

In this work, we expose bilayer graphene to oxygen molecules, and we are able to asymmetrically tune the hole and electron mobilities. These effects reveal that two different sources of carrier scattering are being observed: hole mobility is mainly affected by the long-range scattering process (mainly induced from the underlying substrate) and increases due to the screening promoted by oxygen molecules trapped between the graphene and the substrate. On the other hand, electron transport is strongly sensitive to short-range scattering due to resonant oxygen states located above the charge neutrality point (CNP). Our theoretical calculations demonstrate that the electron coupling with such resonant states is mainly responsible for suppression of the electron mobility, resulting in an asymmetry between electron and hole charge transport. Additionally, a phenomenological model was proposed to assess the contribution of both scattering processes on the hole and electron mobilities. These understandings are fundamental for

* Address correspondence to rlacerda@fisica.ufmg.br.

Received for review December 25, 2012 and accepted July 16, 2013.

Published online July 16, 2013
10.1021/nn402653b

a better control over graphene charge scattering mechanisms and may lead to novel manipulations of its electrical properties.[23,24]

RESULTS AND DISCUSSION

A systematic study of the effect of adsorption and desorption of oxygen is realized at a constant temperature of 150 °C. As an initial conditioning, we flow ultrahigh purity Ar (650 sccm) for 7 h until the CNP position becomes fixed; due to doping from thermally activated defects on the SiO_2 surface, the CNP usually stays at −50 V with intrinsic charging of $n = 3.6 \times 10^{12}$ cm^{-2}. After reaching this stationary situation, we insert a flow of 5% of ultrahigh purity O_2, keeping the total gas flow constant. Figure 1a depicts a diagram of the bilayer device exposed to oxygen molecules. As observed in Figure 1b, as soon as oxygen starts to flow, both charge density and carrier mobility start to change. The charge neutrality point shifts toward zero gate voltage (V_G), the p-type carrier mobility increases from 600 to about 1200 cm^2/V·s, and the electron mobility decreases from 1800 to about 1450 cm^2/V·s (see Figure 2c,d). The measurements are performed as a function of time until a saturation point is reached (∼160 min), and no further change in the electrical properties of the sample are observed. For simplicity, we will refer to these sets of measurements as oxygen *adsorption*. When the O_2 flow is stopped, the reverse effect occurs. The oxygen molecules continuously desorb from the sample, and the system is restored to its initial condition (Figure 1c). Again, for simplicity, we will refer to this stage as *desorption*. As it will be discussed later, this process is generally longer than the first one, and both the mobility and the intrinsic doping of the sample return to the initial conditions. This reversibility suggests that neither oxidation nor formation of permanent epoxy groups (C−O) occurs. Indeed, we confirm the integrity of graphene by performing Raman spectroscopy after the electrical measurements, and no significant defective D peak is observed (see Supporting Information).

Figure 2a depicts in detail the reversible behavior of the CNP position during oxygen adsorption and desorption at 150 °C. For a better understanding of this behavior, we perform a series of adsorption experiments at different temperatures, as shown in Figure 2b. At room temperature (and up to 70 °C), there is only a slight interaction between oxygen and bilayer

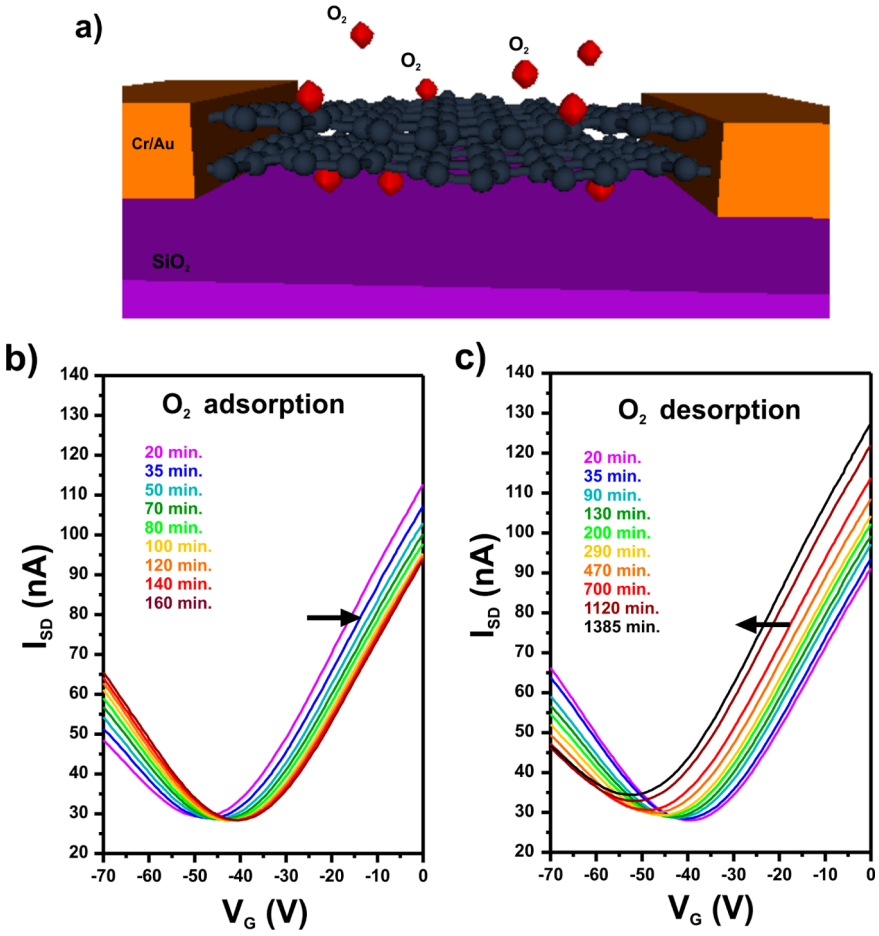

Figure 1. (a) Diagram of the bilayer graphene device exposed to oxygen molecules. (b,c) Source−drain current (I_{SD}) *versus* gate voltage (V_G) as a function of time in the adsorption and desorption process of O_2 on bilayer graphene at 150 °C.

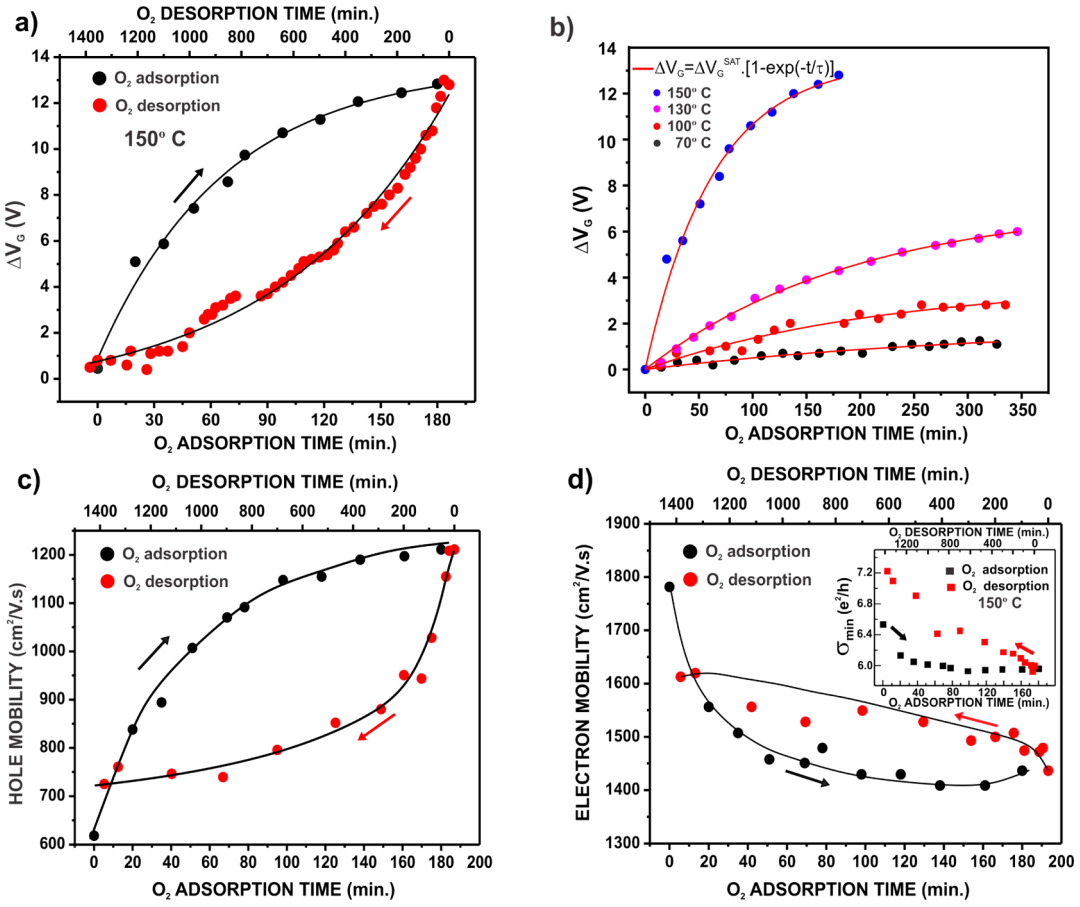

Figure 2. Changes in the electrical properties of a bilayer graphene as a function of time due to the interaction with O_2 molecules. (a) Shift in the charge neutrality point as a function of O_2 adsorption and desorption. (b) Shift in the charge neutrality point as a function of O_2 adsorption at different temperatures. The fitting shown by the red lines refers to the first-order Langmuir-type adsorption model (see Supporting Information for details). (c,d) Electron and hole mobility changes as a function of the (de)adsorption of O_2 molecules. The inset shows the reversible behavior of the minimum of conductivity. Black lines shown in (a), (c), and (d) are a guide for the eyes.

graphene. Interestingly, as the temperature increases, the shift of the CNP becomes more evident, indicating a thermally activated process. Finally, we present the hole and electron mobility changes, as well as the reversible behavior of the minimum of conductivity at the CNP (see inset in Figure 2d) in the adsorption and desorption processes. As noted in Figure 2c,d, by exposing to oxygen molecules, we observe a significant *increase* in hole mobility and a *decrease* in electron mobility on bilayer graphene. The field effect mobility was assumed to be gate-independent and estimated according to $\mu = (d\sigma/dV_g) \times (c_g)^{-1}$, where c_g is the back gate capacitance per unit area, away from the neutrality point. We will also be referring to the expressions p-type ($V_G - V_{CNP} < 0$) and n-type ($V_G - V_{CNP} > 0$) for the electrostatic doping.

Figure 2a demonstrates the kinetics of the interaction between bilayer graphene and oxygen molecules. The first feature to be noted is that the p-type charge transfer resulting from such interaction saturates at a certain level, indicating that there is a limited number of O_2 interaction sites within the bilayer graphene device. This behavior can be described by a first-order Langmuir-type adsorption model (see Supporting Information for details). In addition, the time scale for saturation is rather large, on the order of tens of minutes. This suggests that the observed charge transfer cannot be attributed to a simple O_2 physisorption because saturation of physisorption sites should occur very rapidly under the large O_2 partial pressure (~0.05 atm) used in our experiments.[25,26] Moreover, it is well-known that O_2 physisorption on basal graphite surfaces or single-walled carbon nanotubes (SWCNTs) does not result in charge transfer.[27,28] On the other hand, the changes due to O_2 exposition observed in our experiments are fully reversible and do not generate defective sp^2-bonded sites, according to the nonexistence of a D-band in the Raman spectra of the exposed devices. Thus, no evidence is found for O_2 chemisorption at the graphene surfaces (such as C oxidation or O_2 dissociation followed by formation of epoxy groups), and any O_2 chemisorption that might be favored at the contact metal/graphene interface[29] does not significantly affect device properties.[16]

The interpretation that O_2 physisorbed at the uncovered graphene surface does not contribute to hole

doping is also corroborated by the temperature dependence of the adsorption curves shown in Figure 2b. If O_2 physisorption would result in doping, then, upon heating, one would expect a decrease in such effect because the adsorption/desorption balance would be shifted to the desorption side; that is, the number of occupied interaction sites would be reduced. However, the O_2 doping increases when temperature is increased, as it is clearly demonstrated in Figure 2b. Therefore, this combined evidence suggests that the active O_2 interaction sites (*i.e.*, interaction that leads to charge transfer and thus doping) are located *within the graphene/SiO_2 interface* and not in the uncovered graphene surface. By performing *in situ* Raman measurements, Ryu *et al.* have observed similar reversible hole doping upon O_2 exposure of single-layer graphene on SiO_2 substrates.[24] The authors attributed the effect to charge transfer from O_2 molecules within the graphene/SiO_2 interface. They derived one possible explanation from the work of Shamir *et al.*, which has shown that O_2 and other gases can be electrostatically attracted by charge accumulated on the silicon dioxide surface.[30] In a second step, such a bound O_2 molecule could act as an acceptor center and thus promote the hole doping by partial charge transfer from graphene and simultaneously affect the electron and hole mobilities as it will be discussed next.

The origin of the scattering mechanisms in devices with graphene on SiO_2 substrates has been subject to intense scrutiny.[31−33] Several experimental approaches have been attempted, especially in monolayer graphene, in order to identify the source of carrier scattering, including transport measurements at different dielectric environments or upon exposure to different molecules.[7,8,13,14,16] Particularly, two scattering models have been evoked in the interpretation of these experimental results, *viz.*, charged long-range impurity scattering[34] and resonant short-range impurity scattering.[35−37] However, there is still controversy regarding whether each model can provide a broad and unique explanation for the carrier transport within such devices. In spite of this lack of consensus, it is usually agreed that charged (long-range) scattering would be the dominant mechanism for "dirty" low mobility samples, whereas short-range scattering caused by adatoms, defects, or rippling would be the principal mechanism for "clean" high mobility samples.[10,11] One way to address these issues was performed by Fuhrer's group, where charged impurity scattering was verified experimentally by exposing monolayer graphene to potassium ions (K).[7] In this case, an excellent agreement between experiment and Boltzmann's theory regarding long-range charged impurity scattering was obtained. A similar work, performed by the same group, for bilayer graphene also provided evidence for charged impurity scattering; however, the authors suggested that the full explanation of the experimental data required other sources of scattering (such as short-range) to be taken into account.[17]

In this context, our work shows that the exposure of bilayer graphene to oxygen molecules generates an asymmetrical change in the electron and hole mobilities, revealing that two different sources of carrier scattering are being observed. As previously discussed, the O_2 molecules are incorporated between the bottom graphene layer and the substrate, probably binding to specific SiO_2 sites created by the temperature annealing process. This interfacial O_2 may influence the bilayer graphene electrical properties by (1) decreasing the role of scatterers such as substrate defects, corrugation, or charged impurities by acting as a screening center as theoretically predicted by Huang and Das Sarma;[38,39] (2) possibly increasing the average distance between the substrate impurities and graphene carriers. Nevertheless, it is to be noted that both of these effects would contribute to an increase in the mobility for both p-type and n-type electrostatic doping.

Another scattering source comes from a resonant mechanism, in which a defect (impurity, adatom, and so on) adds electronic levels near the charge neutrality point.[35−37] To evaluate the importance of this mechanism to the present case, we have carried out spin-polarized band structure calculations based on the pseudopotential density functional theory[40,41] as implemented in the SIESTA program[42] and within a recently introduced exchange-correlation functional which takes into account van der Waals interactions in a self-consistent way.[43−45] Our model system consists of a reconstructed O-terminated SiO_2 slab representing the 001 surface of alpha-quartz on top of which we placed a bilayer graphene.[46] The commensurability mismatches are minor within this model, never exceeding 0.3% considering the isolated bilayer graphene calculation (fully relaxed) as reference. Oxygen molecules are included in the interfacial region as well as on the top of the bilayer graphene. An extended cell (for visualization purposes) of the fully relaxed geometry is shown in Figure 3a, and the corresponding band structure is presented in the left panel of Figure 3b, with the Fermi level represented by a dashed line at zero energy (see Supporting Information for a complete visualization of the band structure including spin polarization). It is clear in the figure that the oxygen molecules introduce a set of less dispersive states above and close to the Fermi level, which become more mixed with carbon states in the CNP region. This latter feature may be seen in the projected density of states shown in the right panel of Figure 3b and in the zoomed image around the CNP presented in the top inset. There is a certain degree of hybridization between O and C orbitals, mainly for positive energies, an effect that rapidly decays for energies below the Fermi level, indicating the importance of a resonant

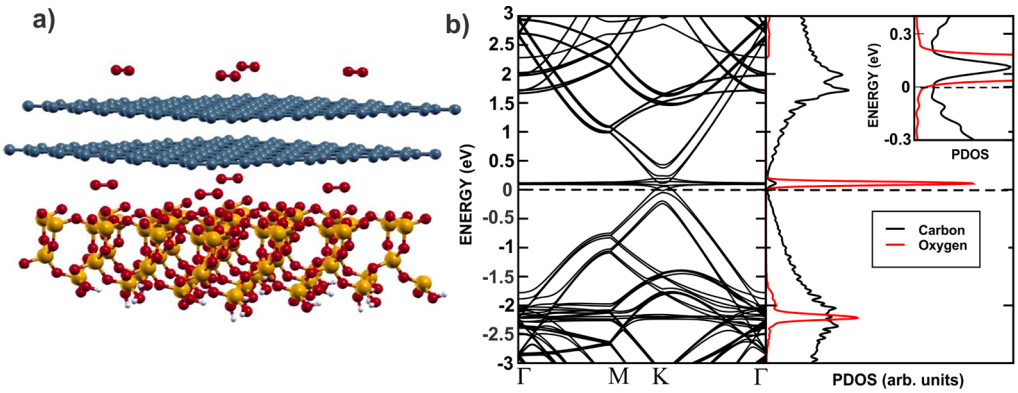

Figure 3. (a) Extended cell showing the relaxed structure of the model system employed with a reconstructed SiO_2 slab and oxygen molecules incorporated above and below the bilayer. Gray, orange, red, and white spheres represent carbon, silicon, oxygen, and hydrogen atoms, respectively. (b) Left panel: Band structure of the system described in (a). For visualization purposes, we did not distinguish the two spin components. The Fermi level is indicated by a dashed line. Right panel: Projected density of states with black and red lines for carbon and oxygen contributions, respectively. The inset shows a zoomed image around the Fermi level. A broadening in the PDOS of 0.03 eV was employed for visualization purposes.

scattering mechanism for a n-doped system. In other words, the orbital mixing found above the CNP is a source of resonant scattering, which contributes to the experimentally observed decrease of the n-type mobility in this energy range, while the states below the CNP are mainly C-type, making the O contribution negligible in the description. Essentially, the same phenomenology is observed when we employ a simpler model in which the substrate is removed and only the oxygen molecules are present. However, the presence of the substrate is important to understand the observed increase in the p-type mobility in the experimental data. Indeed, as previously discussed, this effect may be ascribed to the incorporation of oxygen molecules in the interfacial region, acting, for instance, as screening centers. In accordance with our results, Ferreira *et al.* recently reported a unified model for graphene and bilayer graphene transport based on resonant scatterers, where it has been suggested that the origin of such scatterers would lie in adsorbed hydrocarbons at the graphene surface.[37] Additionally, Wehling *et al.* theoretically predicted that if such a resonant state is created above/below the CNP, an asymmetry between electron and hole mobility would be expected.[35]

To further provide an assessment of the contribution of both short-range and long-range scattering on the electron and hole mobilities, we now present a model that includes both scattering mechanisms and allows for a fitting of our experimental results. First, we recall our main hypotheses: (i) oxygen adsorption in the interfacial region contributes to an increase in the electron and hole mobilities due to screening of substrate impurities, and (ii) resonant states, evidenced in our DFT calculations for energies above the CNP, are responsible for a decrease in electron mobility, an effect that competes with the increased trend originated from the mechanism described in point (i). Interestingly, if the same experiment was to be performed on suspended graphene devices, the resonant effect caused by the oxygen molecules would induce a decrease of only the electron mobility, keeping the hole mobility unchanged. It is also important to recall that both the long-range charge impurity model proposed by Das Sarma *et al.*[18] and the resonant short-range scattering proposed by Ferreira *et al.*[37] result in conductivities of bilayer graphene that are linear with the carrier density ($\sigma \propto n$) and mobilities that are independent of the carrier concentration and inversely proportional to the impurity concentration, leading to $\mu = C/N_{imp}$.

As already described (see Supporting Information for details), a Langmuir-type adsorption model was employed to describe the kinetics of oxygen adsorption, leading to a CNP shift given by $\Delta V_G = \Delta V_G^{SAT}(1 - e^{-t/\tau})$. Applying point (i) of our theoretical model, we expect that the number of long-range impurities (N_{imp}) is a function of time and given by the sum of two contributions: substrate impurities (N_{SiO_2}), which would decrease at the same rate as the O_2 uptake ($dV_G/dt = (1/\tau)e^{-t/\tau}$), and oxygen impurities (N_{O_2}), with a saturation value $N_{O_2}^{SAT}$. According to refs 17 and 18, we can directly correlate the shift in CNP (ΔV_G) to the number of adsorbed oxygen impurities by $N_{O_2} = (c_g/e)\Delta V_G$. Thus, the time dependence of the oxygen impurities would be given by $N_{O_2} = N_{O_2}^{SAT}(1 - e^{-t/\tau})$, which is shown as a fitting to the experimental results in Figure 4a. Therefore, the total impurity concentration would be

$$N_{imp} = N_{SiO_2}^0 e^{-t/\tau} + N_{O_2}^{SAT}(1 - e^{-t/\tau}) \quad (1)$$

where $N_{SiO_2}^0$ is the initial impurity value of the SiO_2 substrate. Thus, introducing N_{imp} on the relation, $\mu = C/N_{imp}$, we obtain the following expression for the hole mobility:

$$\mu_h = \frac{C}{N_{SiO2}^0 e^{-t/\tau} + N_{O_2}^{SAT}(1 - e^{-t/\tau})} = \frac{1}{Ae^{-t/\tau} + B(1 - e^{-t/\tau})} \quad (2)$$

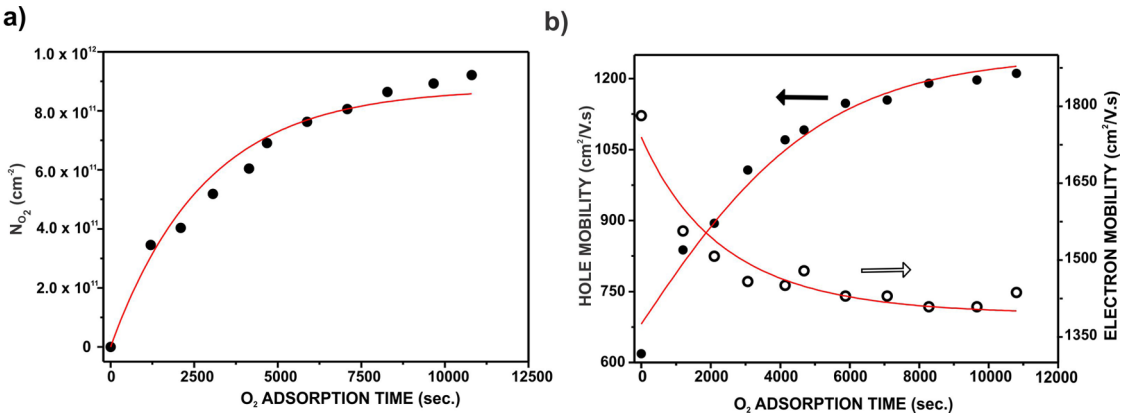

Figure 4. (a) Time dependence of the adsorbed oxygen impurities as a function of time. The fitting procedure was executed based on the equation $N_{O_2} = N_{O_2}^{SAT}(1 - e^{-t/\tau})$. (b) Hole mobility and electron mobility as a function of oxygen adsorption time. Fitting procedures were performed using eqs 2 and 3.

Figure 4b depicts eq 2 fitted to the experimental results for the hole mobility. We emphasize that the same value of τ obtained from the N_{O_2} fitting was used in eq 2, so that we were left with only two fitting parameters. Additionally, the value obtained for constant C ($\sim 10^{15}$ $(V \cdot s)^{-1}$) has the same order of magnitude as other values found in the literature.[6,17,39]

Next, we turn to the time dependence of the electron mobility. According to our theoretical model, there is a resonant scattering mechanism superimposed to a long-range charged impurity scattering, so that we apply Matthiessen's rule to write

$$\frac{1}{\mu_e} = \frac{1}{\mu_c} + \frac{1}{\mu_R} \tag{3}$$

in which μ_c and μ_R stand for the mobilities originated from the charged impurity and the resonant scattering mechanisms, respectively. The former has the same time dependence discussed before, and the latter accompanies the time dependence of the oxygen adsorption, so that we write

$$\mu_c = \frac{D}{Ae^{-t/\tau} + B(1 - e^{-t/\tau})} \tag{4}$$

$$\mu_R = \frac{E}{(1 - e^{-t/\tau})} \tag{5}$$

in which A, B, and τ are the same as before, and D and E are the proportionality constants related to μ_c and μ_R, respectively (D must be included due to the different scattering cross sections of electrons and hole carriers). Again, Figure 4b shows that the resulting equation fitted very well the experimental data (with only two additional fitting parameters, D and E). A similar procedure was performed for the desorption process, providing approximately the same results for the fitting parameters (see Supporting Information for details).

Based on the results of the fittings made with the above model, it becomes clear that we can only explain the behavior of the electron mobility if we take into consideration both types of scattering mechanisms (long- and short-range), providing further support for the asymmetric behavior of the O_2 resonant centers. Thus, our theoretical and experimental results clearly demonstrate that adsorbed species (from an external source) can play the role of short-range scatterers and that they can also asymmetrically affect the electron and hole mobilities.

CONCLUSIONS

Our experiments and theoretical calculations demonstrate that the adsorption of oxygen molecules on graphene has two distinct effects on electron and hole mobilities: (1) the adsorbed molecules originate impurity resonances at energies higher than that of CNP, which results in asymmetry between electron and hole mobilities; (2) the molecules also provide a screening effect for existing long-range scatterers at the underlying substrate *via* incorporation of oxygen molecules at the interfacial region between the substrate and the bilayer.

EXPERIMENTAL METHODS

We deposit bilayer graphene *via* standard mechanical exfoliation of graphite on top of 300 nm SiO_2 grown on heavily doped p-type Si substrates. The number of layers and the AB staking order are precisely confirmed by Raman spectroscopy and optical contrast.[47] Contacts of Cr/Au (3/35 nm) are fabricated by standard electron beam lithography, producing field effect transistor devices whereby the Si substrate is used as the back gate contact. The device is transferred into a tubular testing chamber, wherein we perform *in situ* electrical measurements probing the charge density of the bilayer graphene by both electrostatically gating and by interacting with O_2 molecules at different temperatures. To verify the reproducibility, the measurements were repeated in more than one device and the same qualitative results were observed (see Supporting Information).

The electronic properties of bilayer graphene are strongly dependent on the state of cleanness of the samples and are also sensitive to adsorbed impurities, its surrounding environment, and temperature.[48] Then, we developed a standard cleaning procedure to perform the experiments. The device is initially submitted to 12 h long thermal annealing at 230 °C with constant flow of Ar/H_2 (10%) to remove PMMA residue reminiscent from the electron beam lithography process. After this procedure, our samples show a better response to the adsorption of oxygen molecules, and typically, the neutrality point gets shifted to the n-type doping region due to the activation of surface defects in the SiO_2 substrate.[49]

Conflict of Interest: The authors declare no competing financial interest.

Acknowledgment. E.A.M., I.S., A.M.B.G., and A.O.M. are thankful to CNPq and CAPES for their scholarships. H.C., M.S.C.M., A.S.F., and R.G.L. are Cnpq fellows. We thank D.E. Alves for helping with the cartoon of Figure 1. Financial support from CAPES, Fapemig, CNPq/MCT, and INCT/Nanomateriais de Carbono is also acknowledged.

Supporting Information Available: Raman scattering for the bilayer graphene device before and after O_2 exposure. Analysis of the normalized conductivity as a function of the carrier density. Kinetics of hole doping upon oxygen exposure which can be described by a first-order Langmuir-type adsorption model. Electron and hole mobilities as a function of O_2 adsorption time at 150 °C for two other devices. Behavior of the monolayer graphene device under oxygen exposure. Phenomenological model for the desorption process. Results of spin-polarized band structure and density of states. This material is available free of charge *via* the Internet at http://pubs.acs.org.

REFERENCES AND NOTES

1. Zhang, Y. B.; Tan, Y. W.; Stormer, H. L.; Kim, P. Experimental Observation of the Quantum Hall Effect and Berry's Phase in Graphene. *Nature* **2005**, *438*, 201–204.
2. Novoselov, K. S.; Geim, A. K.; Morozov, S. V.; Jiang, D.; Zhang, Y.; Dubonos, S. V.; Grigorieva, I. V.; Firsov, A. A. Electric Field Effect in Atomically Thin Carbon Films. *Science* **2004**, *306*, 666–669.
3. Novoselov, K. S.; Geim, A. K.; Morozov, S. V.; Jiang, D.; Katsnelson, M. I.; Grigorieva, I. V.; Dubonos, S. V.; Firsov, A. A. Two-Dimensional Gas of Massless Dirac Fermions in Graphene. *Nature* **2005**, *438*, 197–200.
4. Bolotin, K. I.; Ghahari, F.; Shulman, M. D.; Stormer, H. L.; Kim, P. Observation of the Fractional Quantum Hall Effect in Graphene. *Nature* **2009**, *462*, 196–199.
5. Schedin, F.; Geim, A. K.; Morozov, S. V.; Hill, E. W.; Blake, P.; Katsnelson, M. I.; Novoselov, K. S. Detection of Individual Gas Molecules Adsorbed on Graphene. *Nat. Mater.* **2007**, *6*, 652–655.
6. Chen, F.; Xia, J. L.; Tao, N. J. Ionic Screening of Charged-Impurity Scattering in Graphene. *Nano Lett.* **2009**, *9*, 1621–1625.
7. Chen, J. H.; Jang, C.; Adam, S.; Fuhrer, M. S.; Williams, E. D.; Ishigami, M. Charged-Impurity Scattering in Graphene. *Nat. Phys.* **2008**, *4*, 377–381.
8. Newaz, A. K.; Puzyrev, Y. S.; Wang, B.; Pantelides, S. T.; Bolotin, K. I. Probing Charge Scattering Mechanisms in Suspended Graphene by Varying Its Dielectric Environment. *Nat. Commun.* **2012**, *3*, 734.
9. Chen, J. H.; Jang, C.; Xiao, S. D.; Ishigami, M.; Fuhrer, M. S. Intrinsic and Extrinsic Performance Limits of Graphene Devices on SiO_2. *Nat. Nanotechnol.* **2008**, *3*, 206–209.
10. Castro Neto, A. H.; Guinea, F.; Peres, N. M. R.; Novoselov, K. S.; Geim, A. K. The Electronic Properties of Graphene. *Rev. Mod. Phys.* **2009**, *81*, 109–162.
11. Das Sarma, S.; Adam, S.; Hwang, E. H.; Rossi, E. Electronic Transport in Two-Dimensional Graphene. *Rev. Mod. Phys.* **2011**, *83*, 407–470.
12. Mucciolo, E. R.; Lewenkopf, C. H. Disorder and Electronic Transport in Graphene. *J. Phys.: Condens. Matter* **2010**, *22*, 273201.
13. Ponomarenko, L. A.; Yang, R.; Mohiuddin, T. M.; Katsnelson, M. I.; Novoselov, K. S.; Morozov, S. V.; Zhukov, A. A.; Schedin, F.; Hill, E. W.; Geim, A. K. Effect of a High-Kappa Environment on Charge Carrier Mobility in Graphene. *Phys. Rev. Lett.* **2009**, *102*, 206603.
14. Katoch, J.; Chen, J. H.; Tsuchikawa, R.; Smith, C. W.; Mucciolo, E. R.; Ishigami, M. Uncovering the Dominant Scatterer in Graphene Sheets on SiO_2. *Phys. Rev. B* **2010**, *82*, 081417.
15. Dan, Y. P.; Lu, Y.; Kybert, N. J.; Luo, Z. T.; Johnson, A. T. C. Intrinsic Response of Graphene Vapor Sensors. *Nano Lett.* **2009**, *9*, 1472–1475.
16. Farmer, D. B.; Golizadeh-Mojarad, R.; Perebeinos, V.; Lin, Y. M.; Tulevski, G. S.; Tsang, J. C.; Avouris, P. Chemical Doping and Electron–Hole Conduction Asymmetry in Graphene Devices. *Nano Lett.* **2009**, *9*, 388–392.
17. Xiao, S. D.; Chen, J. H.; Adam, S.; Williams, E. D.; Fuhrer, M. S. Charged Impurity Scattering in Bilayer Graphene. *Phys. Rev. B* **2010**, *82*, 041406(R).
18. Adam, S.; Das Sarma, S. Boltzmann Transport and Residual Conductivity in Bilayer Graphene. *Phys. Rev. B* **2008**, *77*, 115436.
19. Castro, E. V.; Novoselov, K. S.; Morozov, S. V.; Peres, N. M. R.; Dos Santos, J.; Nilsson, J.; Guinea, F.; Geim, A. K.; Neto, A. H. C. Biased Bilayer Graphene: Semiconductor with a Gap Tunable by the Electric Field Effect. *Phys. Rev. Lett.* **2007**, *99*, 216802.
20. Zhang, Y. B.; Tang, T. T.; Girit, C.; Hao, Z.; Martin, M. C.; Zettl, A.; Crommie, M. F.; Shen, Y. R.; Wang, F. Direct Observation of a Widely Tunable Bandgap in Bilayer Graphene. *Nature* **2009**, *459*, 820–823.
21. Yacoby, A. Graphene: Tri and Tri Again. *Nat. Phys.* **2011**, *7*, 925–926.
22. Lui, C.; Hung, Li, Z.; Mak, K. F.; Cappelluti, E.; Heinz, T. F. Observation of an Electrically Tunable Band Gap in Trilayer Graphene. *Nat. Phys.* **2011**, *7*, 944–947.
23. Zhang, W. J.; Lin, C. T.; Liu, K. K.; Tite, T.; Su, C. Y.; Chang, C. H.; Lee, Y. H.; Chu, C. W.; Wei, K. H.; Kuo, J. L.; *et al.* Opening an Electrical Band Gap of Bilayer Graphene with Molecular Doping. *ACS Nano* **2011**, *5*, 7517–7524.
24. Ryu, S.; Liu, L.; Berciaud, S.; Yu, Y. J.; Liu, H. T.; Kim, P.; Flynn, G. W.; Brus, L. E. Atmospheric Oxygen Binding and Hole Doping in Deformed Graphene on a SiO_2 Substrate. *Nano Lett.* **2010**, *10*, 4944–4951.
25. Sato, Y.; Takai, K.; Enoki, T. Electrically Controlled Adsorption of Oxygen in Bilayer Graphene Devices. *Nano Lett.* **2011**, *11*, 3468–3475.
26. Yang, Y.; Murali, R. Binding Mechanisms of Molecular Oxygen and Moisture to Graphene. *Appl. Phys. Lett.* **2011**, *98*, 093116.
27. Ulbricht, H.; Moos, G.; Hertel, T. Physisorption of Molecular Oxygen on Single-Wall Carbon Nanotube Bundles and Graphite. *Phys. Rev. B* **2002**, *66*, 075404.
28. Levesque, P. L.; Sabri, S. S.; Aguirre, C. M.; Guillemette, J.; Siaj, M.; Desjardins, P.; Szkopek, T.; Martel, R. Probing Charge Transfer at Surfaces Using Graphene Transistors. *Nano Lett.* **2011**, *11*, 132–137.
29. Dai, J.; Yuan, J. Adsorption of Molecular Oxygen on Doped Graphene: Atomic, Electronic, and Magnetic Properties. *Phys. Rev. B* **2010**, *81*, 165414.
30. Shamir, N.; Mihaychuk, J. G.; van Driel, H. M.; Kreuzer, H. J. Universal Mechanism for Gas Adsorption and Electron Trapping on Oxidized Silicon. *Phys. Rev. Lett.* **1999**, *82*, 359–361.
31. Stauber, T.; Peres, N. M. R.; Guinea, F. Electronic Transport in Graphene: A Semiclassical Approach Including Midgap States. *Phys. Rev. B* **2007**, *76*, 205423.
32. Tan, Y. W.; Zhang, Y.; Bolotin, K.; Zhao, Y.; Adam, S.; Hwang, E. H.; Das Sarma, S.; Stormer, H. L.; Kim, P. Measurement of Scattering Rate and Minimum Conductivity in Graphene. *Phys. Rev. Lett.* **2007**, *99*, 246803.
33. Monteverde, M.; Ojeda-Aristizabal, C.; Weil, R.; Bennaceur, K.; Ferrier, M.; Gueron, S.; Glattli, C.; Bouchiat, H.; Fuchs, J. N.; Maslov, D. L. Transport and Elastic Scattering Times as Probes of the Nature of Impurity Scattering in Single-Layer and Bilayer Graphene. *Phys. Rev. Lett.* **2010**, *104*, 126801.

34. Rossi, E.; Das Sarma, S. Ground State of Graphene in the Presence of Random Charged Impurities. *Phys. Rev. Lett.* **2008**, *101*, 166803.
35. Wehling, T. O.; Yuan, S.; Lichtenstein, A. I.; Geim, A. K.; Katsnelson, M. I. Resonant Scattering by Realistic Impurities in Graphene. *Phys. Rev. Lett.* **2010**, *105*, 056802.
36. Ni, Z. H.; Ponomarenko, L. A.; Nair, R. R.; Yang, R.; Anissimova, S.; Grigorieva, I. V.; Schedin, F.; Blake, P.; Shen, Z. X.; Hill, E. H.; *et al.* On Resonant Scatterers as a Factor Limiting Carrier Mobility in Graphene. *Nano Lett.* **2010**, *10*, 3868–3872.
37. Ferreira, A.; Viana-Gomes, J.; Nilsson, J.; Mucciolo, E.; Peres, N.; Castro Neto, A. Unified Description of the DC Conductivity of Monolayer and Bilayer Graphene at Finite Densities Based on Resonant Scatterers. *Phys. Rev. B* **2011**, *83*, 165402.
38. Hwang, E. H.; Adam, S.; Das Sarma, S. Transport in Chemically Doped Graphene in the Presence of Adsorbed Molecules. *Phys. Rev. B* **2007**, *76*, 195421.
39. Zhang, W.; Li, L.-J. The Screening of Charged Impurities in Bilayer Graphene. *New J. Phys.* **2010**, *12*, 103037.
40. Kohn, W.; Sham, L. J. Self-Consistent Equations Including Exchange and Correlation Effects. *Phys. Rev.* **1965**, *140*, A1133.
41. Kleinman, L.; Bylander, D. M. Efficacious Form for Model Pseudopotentials. *Phys. Rev. Lett.* **1982**, *48*, 1425–1428.
42. Soler, J. M.; Artacho, E.; Gale, J. D.; Garcia, A.; Junquera, J.; Ordejón, P.; Sanchez-Portal, D. The SIESTA Method for *Ab Initio* Order-N Materials Simulation. *J. Phys.: Condens. Matter* **2002**, *14*, 2745.
43. Dion, M.; Rydberg, H.; Schröder, E.; Langreth, D. C.; Lundqvist, B. I. van der Waals Density Functional for General Geometries. *Phys. Rev. Lett.* **2004**, *92*, 246401.
44. Thonhauser, T.; Cooper, V. R.; Li, S.; Puzder, A.; Hyldgaard, P.; Langreth, D. C. van der Waals Density Functional: Self-Consistent Potential and the Nature of the van der Waals Bond. *Phys. Rev. B* **2007**, *76*, 125112.
45. Román-Pérez, G.; Soler, J. M. Efficient Implementation of a van der Waals Density Functional: Application to Double-Wall Carbon Nanotubes. *Phys. Rev. Lett.* **2009**, *103*, 096102.
46. Nguyen, T. C.; Otani, M.; Okada, S. Semiconducting Electronic Property of Graphene Adsorbed on (0001) Surfaces of SiO_2. *Phys. Rev. Lett.* **2011**, *106*, 106801.
47. Ferrari, A. C.; Meyer, J. C.; Scardaci, V.; Casiraghi, C.; Lazzeri, M.; Mauri, F.; Piscanec, S.; Jiang, D.; Novoselov, K. S.; Roth, S.; *et al.* Raman Spectrum of Graphene and Graphene Layers. *Phys. Rev. Lett.* **2006**, *97*, 187401.
48. Dan, Y. P.; Lu, Y.; Kybert, N. J.; Luo, Z. T.; Johnson, A. T. C. Intrinsic Response of Graphene Vapor Sensors. *Nano Lett.* **2009**, *9*, 1472–1475.
49. Romero, H. E.; Shen, N.; Joshi, P.; Gutierrez, H. R.; Tadigadapa, S. A.; Sofo, J. O.; Eklund, P. C. n-Type Behavior of Graphene Supported on Si/SiO_2 Substrates. *ACS Nano* **2008**, *2*, 2037–2044.